Free Radical Biology and Medicine 99 (2016) 286–295

Contents lists available at ScienceDirect

Free Radical Biology and Medicine

journal homepage: www.elsevier.com/locate/freeradbiomed

Suppression of StarD7 promotes endoplasmic reticulum stress and induces ROS production

Jésica Flores-Martín, Luciana Reyna, Magali E. Ridano, Graciela M. Panzetta-Dutari, Susana Genti-Raimondi *

Universidad Nacional de Córdoba-Consejo Nacional de Investigaciones Científicas y Técnicas, Facultad de Ciencias Químicas, Departamento de Bioquímica Clínica-Centro de Investigaciones en Bioquímica Clínica e Inmunología, Haya de la Torre y Medina Allende, X5000HUA Córdoba, Argentina

ARTICLE INFO

Article history:
Received 11 March 2016
Received in revised form
29 July 2016
Accepted 17 August 2016
Available online 20 August 2016

Keywords:
StarD7
START domain
Endoplasmic reticulum stress
Reactive oxygen species
HepG2 cells

ABSTRACT

StarD7 is an intracellular lipid transport protein identified as up-regulated in the choriocarcinoma JEG-3 cell line. StarD7 facilitates the delivery of phosphatidylcholine (PC) to the mitochondria, and StarD7 knockdown causes a reduction in phospholipid synthesis. Since inhibition of PC synthesis may lead to endoplasmic reticulum (ER) stress we hypothesized that StarD7 may be involved in maintaining cell homeostasis. Here, we examined the effect of StarD7 silencing on ER stress response and on the levels of reactive oxygen species (ROS) in the human hepatoma cell line HepG2. StarD7 knockdown induced alterations in mitochondria and ER morphology. These changes were accompanied with an ER stress response as determined by increased expression of inositol-requiring enzyme 1α (IRE1α), calnexin, glucose regulated protein 78/immunoglobulin heavy chain-binding protein (Grp78/BiP), protein kinase-like ER kinase (PERK) as well as the phosphorylated eukaryotic translation initiation factor 2, subunit 1α (p-eIF2α). Additionally, a downregulation of the tumor suppressor p53 by a degradation mechanism was observed in StarD7 siRNA cells. Furthermore, StarD7 silencing induced ROS generation and reduced cell viability after H_2O_2 exposure. Decreased expression of StarD7 was associated to increased levels of the heme oxygenase-1 (HO-1) and catalase enzymes as well as in catalase enzymatic activity. Finally, no changes in levels of autophagy and apoptosis markers were observed in StarD7 siRNA treated cells respect to control cells. Taken together, these results indicate that StarD7 contributes to modulate cellular redox homeostasis.

1. Introduction

StarD7 belongs to the family of START proteins ubiquitously expressed, which are implicated in lipid transport, metabolism, and signaling [1,2]. StarD7 mRNA was first identified using differential display techniques as a JEG-3 over-expressed gene compared with normal and benign trophoblastic samples [3,4]. Semiquantitative RT-PCR assays performed in a series of cell lines have shown that StarD7 has widespread expression, predominantly in trophoblast-derived JEG-3, JAR, and HTR8/SVneo cells, as well as in hepatocellular carcinoma HepG2 cells, colorectal adenocarcinoma HT29 and Caco-2 cells [3,4]. Horibata and Sugimoto demonstrated that StarD7 facilitates the delivery of phosphatidylcholine (PC) to the mitochondria in hepatoma HEPA-1 cells, and suggested that StarD7 extracts PC from the cytoplasmic surface of the ER, Golgi apparatus, or plasma membrane [5]. In addition, we have reported that StarD7 siRNA-transfected JEG-3 cells show decreased phospholipid biosynthesis and ABCG2 expression as well as a reduction in cell migration and proliferation. These observations were accompanied by higher expression of biochemical and morphological differentiation markers [6]. Furthermore, StarD7 gene promoter is activated by Wnt/β-catenin signaling [7], a pathway that promotes proliferation and is frequently altered in cancer cells. Consistently, Ikeda et al. found that miR-193b inhibits pancreatic cancer cell proliferation

Abbreviations: BSA, bovine serum albumin; CHX, cycloheximide; DMSO, dimethyl sulfoxide; ER, endoplasmic reticulum; eIF2α, eukaryotic translation initiation factor 2, subunit 1α; GRP78/BiP, glucose regulated protein 78/immunoglobulin heavy chain-binding protein; H2DCFDA, 2′,7′-dichlorodihydrofluorescein diacetate; H_2O_2, hydrogen peroxide; HO-1, heme oxygenase-1; IRE1α, inositol-requiring enzyme 1; LC3, microtubule-associated protein light chain 3; MTT, 3-(4,5-dimethylthiazol-2yl)-2, 5-diphenyltetrazolium bromide; PBS, phosphate buffered saline; PBST, phosphate buffered saline plus triton X-100; PC, phophatidylcholine; p-eIF2α, phosphorylated eukaryotic translation initiation factor 2, subunit 1α; PERK, protein kinase-like ER kinase; PI, propidium iodide; qRT-PCR, quantitative reverse transcription polymerase chain reaction; ROS, reactive oxygen species; TBS, Tris buffered saline; UPR, unfolded protein response; siC, scrambled siRNA; siD7, StarD7 siRNA; StarD7, StAR related START domain containing 7

* Corresponding author.
E-mail address: sgenti@fcq.unc.edu.ar (S. Genti-Raimondi).

http://dx.doi.org/10.1016/j.freeradbiomed.2016.08.023
0891-5849/

concomitantly with its ability to target and downregulate StarD7 transcript expression [8]. Additionally, genome wide analysis has shown that StarD7 transcript levels are altered in various conditions such as metabolic state, inflammation processes, and cancer suggesting that its expression must be tightly controlled in normal cell physiology [9]. Recently, Yang et al. demonstrated that the viability of StarD7$^{-/-}$ embryos was dramatically decreased after embryonic day 10 highlighting an important role of this protein in development [10].

The endoplasmic reticulum (ER) is a compartment composed of a complex network of tubular and planar membranes where the synthesis and export of proteins, carbohydrates, and lipids take place coordinating diverse signaling pathways that regulate cell metabolism, proliferation and death. PC is the most abundant phospholipid in eukaryotic cell membranes synthesized mainly in the ER. The inhibition of PC synthesis results in altered ER morphology leading to the induction of a regulatory program triggered by ER stress, namely "the unfolded protein response" (UPR) [11,12]. The UPR is an adaptive response composed of three main signaling pathways involving the ER transmembrane sensors: inositol-requiring enzyme 1α (IRE1α), activating transcription factor-6 (ATF6), and protein kinase-like ER kinase (PERK). Each signaling pathway activates transcription factors that mediate the induction of a variety of ER stress response genes connected with ER-associated protein degradation and protein translation attenuation. IRE1α, ATF6 and PERK sense ER stress through Grp78/BiP binding/release via their respective lumenal domains [13]. The UPR inhibits global cap-dependent protein synthesis via PERK-phosphorylated eukaryotic translation initiation factor 2, subunit 1α (p-eIF2α), promotes the upregulation of ER chaperons, and favors the elimination of misfolded proteins via ATF6 and IRE1α. If these adaptive mechanisms are not sufficient to alleviate ER stress, then activation of an apoptotic program involving caspases 7, 12, and 3, JNK, and p53 signaling pathways is initiated [13]. p53 tumor suppressor is a nuclear protein that functions as a regulator of transcription and mediates several biological effects, such as growth arrest, senescence, and apoptosis in response to various forms of stress [14,15]. Depending on the experimental conditions, ER stress was reported to facilitate decreased [16,17] or increased p53 levels or activity [18–21]. Moreover, it was recently reported that p53 regulates ER function in response to stress [22].

Considering the observations that *i)* StarD7 binds PC, *ii)* depletion of StarD7 leads to decreased phospholipid biosynthesis, *iii)* PC synthesis inhibition generates ER stress, and *iv)* StarD7 increased expression is associated with cancer and cell proliferation, we hypothesize that changes in StarD7 expression causes a dysregulation in cellular homeostasis.

In this study, we demonstrate that StarD7 silencing alters mitochondria and ER morphology initiating an UPR pathway concomitant with increased degradation of p53 protein and ROS generation. We speculate that beyond its role in lipid transport, StarD7 contributes to modulate cellular redox homeostasis.

2. Materials and methods

2.1. Antibodies

Mouse monoclonal anti-p-JNK (sc-6254) and anti-JNK (sc-1648); rabbit polyclonal anti-HO-1 (H-105) and goat anti-p53 (FL-393-G) were obtained from Santa Cruz Biotechnology. Rabbit monoclonal anti-phospho-eIF2α (Ser51) (3398) and rabbit polyclonal anti-total-eIF2α (9722) were from Cell Signaling Technology and anti-PARP from Roche. Mouse monoclonal anti-p21 (556,430) was from BD Pharmingen, and mouse monoclonal anti-α-tubulin (Clone B-5-1-2), mouse monoclonal anti-β-actin and rabbit polyclonal anti-LC3 (L1877) were obtained from Sigma Chemical Co. Rabbit polyclonal anti-catalase antibody was from Abcam (ab52477). Anti-StarD7Ct was generated in our laboratory as previously described [4]. All antibodies against ER stress markers (ER Stress Antibody Sampler Kit #9956) were from Cell Signaling Technology. Anti-mouse and anti-rabbit IgG antibodies conjugated to horseradish peroxidase linked F(ab')$_2$ fragment (from sheep or from donkey respectively) were obtained from Amersham Bioscience, and rabbit anti-goat IgG antibody from Zymed. IRDye 800CW donkey anti-rabbit IgG (P/N 096-32213) and IRDye 800CW donkey anti-mouse IgG (P/N 096-32212) were obtained from Li-Cor Biosciences.

2.2. siRNA transfections

HepG2 cells, from a human hepatocellular carcinoma, obtained from American Type Cultured Collections were cultured in Dulbecco's modified Eagle's medium (DMEM), 10% v/v fetal calf serum, 100 μg/μL penicillin, 100 μg/mL streptomycin (Invitrogen). Cells were harvested and seeded either in 6-well plates at 2×10^5 cells/well or in 96-well plates at 1.5×10^4 cells/well and incubated at 37 °C and 5% CO2. After 24 h and at 40% confluence, cells were transfected with 50 nM of one of two specific siRNAs, i.e. siD7 (Sense: GGU AUA GUG UGG AUC AGG ATT and Antisense: UCC UGA UCC ACA CUA UAC CGC; nucleotides 1099-1117, Accession No. NM_020151) or siD7.2 (Sense: GCA CCC ACC UUU ACC AGU ATT and Antisense: UAC UGG UAA AGG UGG GUG CCT, nucleotides 877-895, Accession No. NM_020151) to knockdown endogenous StarD7 expression, or with scrambled negative siRNA as control (Silencer Negative™) (Applied Biosystems/Ambion, Biosystems) and 4 μL of RNAimax (Invitrogen) per mL of OptiMEM. The cells were cultured for 6–72 h and culture medium was refreshed each 24 h. Cultures were conducted in duplicate or in quadruplicate, as indicated, for each set of experiments to assess reproducibility.

2.3. Quantitative reverse transcription PCR (qRT-PCR)

Total RNA was extracted from cultured cells using Trizol (Invitrogen), according to the manufacturer's instructions. Single-stranded cDNAs were synthesized with random primers (Invitrogen) in 20 μL final volume. Briefly, 1 μg of total RNA was incubated with random primers (1.25 ng/μL) and the reverse transcriptase reaction was performed as previously described [3].

For qPCR, cDNA was mixed with SYBR Green PCR Master Mix (Applied Biosystems) and the forward and reverse primers were added to a final volume of 20 μL. Primer sequences and concentration used are listed in Table 1. qPCR was carried out on an Applied Biosystems 7500 Real-Time PCR System with Sequence Detection Software v1.4. The cycling conditions included a hot start at 95 °C for 10 min, followed by 40 cycles at 95 °C for 15 s and 60 °C for 1 min. Specificity was verified by melting curve analysis

Table 1
Primers used for qRT-PCR.

	Sequence (5′–3′)	nM
StarD7		
Sense	GGTAAT CAA GCT GGAGGT GAT TG	100
Antisense	GAG TAC ATT GGA TAA GGA AAA TGG GT	
Cyclophilin A		
Sense	GTC AAC CCC ACC GTG TTC TT	100
Antisense	CTG CTG TCT TTG GGA CCT TGT	
p53		
Sense	CTA GCT CGC TAG TGG GTT GC	300
Antisense	GAA GAC GGC AGC AAA GAA AC	

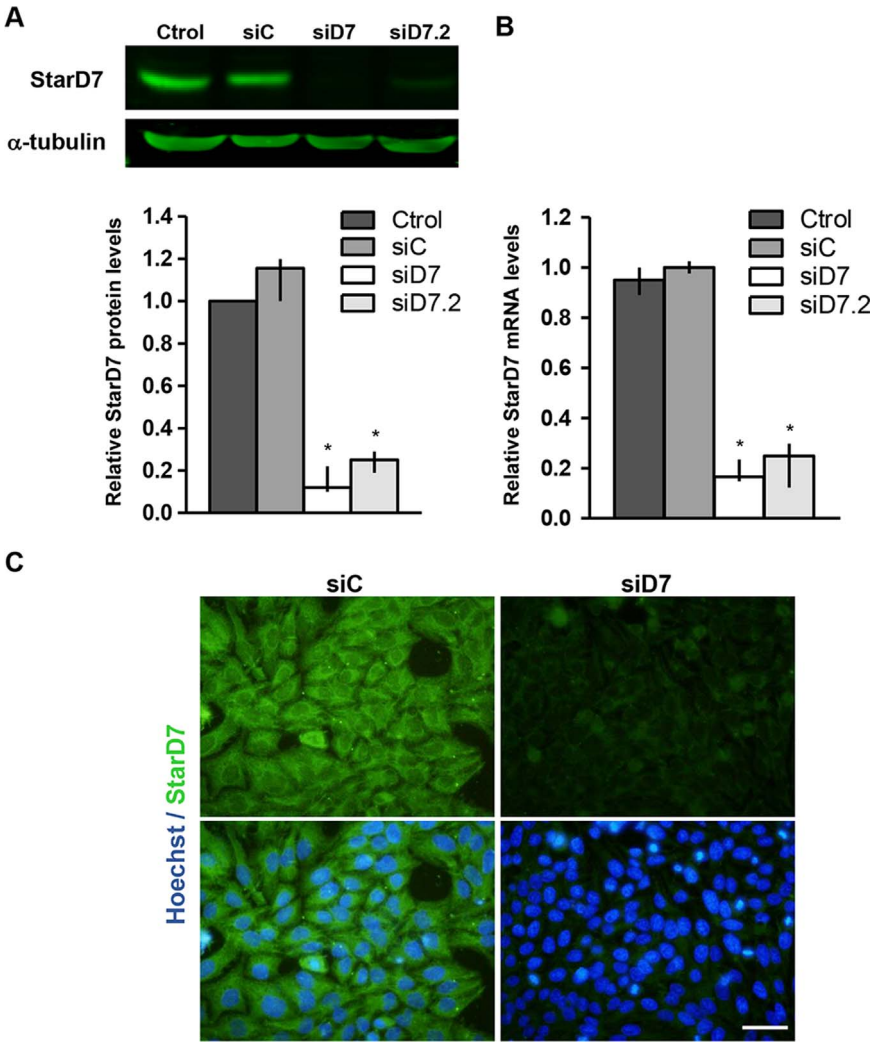

Fig. 1. StarD7 protein and mRNA expression in StarD7-silenced HepG2 cells. Cultured cells were transfected or not with 50 nM of the indicated siRNAs and cultured for 72 h. (A) StarD7 protein expression levels from non-transfected (Ctrol), and siC- or siD7-transfected cells was analyzed by western blot. Filters were incubated with anti-StarD7Ct or anti-α-tubulin antibodies. The bar graph represents the densitometric quantification of StarD7 protein levels in siD7-transfected cells normalized to α-tubulin of five separate experiments relative to the corresponding normalized protein levels in Ctrol cells defined as 1 (median and 25th–75th percentiles). *$p < 0.01$ compared to Ctrol cells. (B) StarD7 expression was determined by qRT-PCR. Results are expressed as fold changes in StarD7 mRNA expression after normalizing to cyclophilin A relative to the corresponding normalized mRNA levels in Ctrol cells. The values represent the median and 25th–75th percentiles of at least three independent experiments performed by triplicate. (C) Epifluorescence microscopy images demonstrating StarD7 expression (green) in siC (left panel) and in siD7-treated cells (right panel). The nuclei were labeled with Hoechst (blue) and merge images are shown on the right. Bar = 20 μm (400 ×).

and agarose gel electrophoresis. Each sample was analyzed in triplicate. Transcript levels were normalized to those of cyclophilin A and relative expression levels were calculated using the $2^{-\Delta\Delta Ct}$ method [23]. Amplification efficiency for each set of primers was near 98%. RNA samples incubated without reverse transcriptase during cDNA synthesis, as well as PCR reactions using water instead of template showed no amplification.

2.4. SDS-PAGE and western blotting

Protein samples were loaded onto 10% SDS-PAGE gels. After migration, proteins were electrotransferred to nitrocellulose (Amersham Bioscience). The membrane was blocked in Tris buffered saline (TBS) (25 mM Tris, 150 mM NaCl, 2 mM KCl, pH 7.4) containing 0.2% w/v Tween-20% and 5% w/v non-fat dry milk, washed and incubated with each one of the following primary antibodies: anti-StarD7Ct (0.5 μg/mL), anti-α-tubulin (1:3000), anti-β-actin (1:3000), anti-p-eIF2α (1:500), anti-total eIF2α (1:500), anti-p21 (1:1000), anti-p53 (1:1000), anti-PARP (1:1000), anti-HO-1 (1:500), anti-pJNK (1:1000), anti-JNK (1:1000), anti-catalase (1:5000), or anti-LC-3 (1:1000) for 1 h at room temperature or overnight 4 °C with shaking, as indicated by the manufactures. The blots for ER stress markers were analyzed with the ER Stress Antibody Sampler Kit (Cell Signaling Technology) according to the manufacturer's instructions.

After washing, the blots were incubated with horseradish peroxidase-conjugated, sheep anti-mouse, or rabbit anti-goat secondary antibodies (1:5000) at room temperature for 1 h. Protein-antibody complexes were visualized by an enhanced chemiluminescence detection system (SuperSignal West Pico; Pierce). Blots were quantified by densitometry using Gel-Pro Analyzer. Alternatively, the blots were incubated with IRDye 800 CW donkey anti-rabbit IG or IRDye 800 CW donkey anti-mouse IgG antibodies (1:15 000) in TBS with 5% w/v BSA for 1 h, protected from light. After washing with TBS plus 0.2% v/v Tween-20, the membranes were visualized and quantified using the Odyssey Infrared Imaging System (LI-COR, Inc., Lincoln, NE, USA). Protein expression was normalized to the α-tubulin expression or β-actin, as indicated.

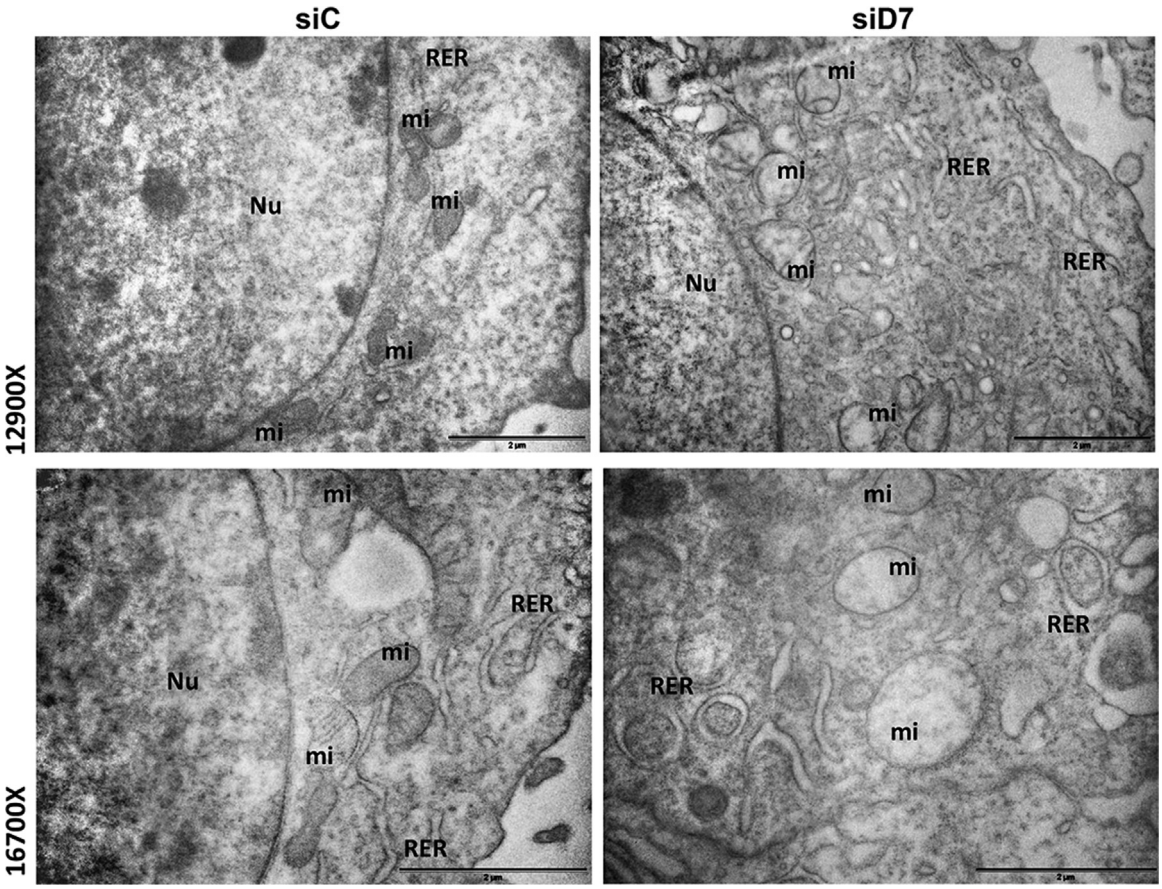

Fig. 2. StarD7 knockdown leads to ultrastructural alterations in HepG2 cells. Cells were transfected with siC (left panels) or siD7 (right panels) and cultured for 72 h. Transmission electron microscopy analysis showed regular cisternae of rough endoplasmic reticulum (RER) under siC conditions but dilated RER cisternae and altered mitochondrias (mi) in siD7-transfected cells. Nu: nucleus. Observations were performed using a Zeiss Leo 906-E electron microscope. Original magnification 12900 × (top panels), 16700 × (bottom panels). Bar = 2 μm.

2.5. Immunofluorescence

HepG2 cells treated with StarD7 siRNA (siD7) or scrambled siRNA (siC) were cultured on coverslips as described above. Cells were fixed 10 min in ice-cold methanol and incubated 10 min with 1 mM ammonium chloride to inhibit quenching. Cells were permeabilized for 7 min with 0.1% Triton X-100 v/v in PBS. Cells were then rinsed with PBS three times, blocked with 2.5% v/v normal goat serum in PBS plus 0.2% v/v Tween-20 (PBST) and with 0.2% w/v fish skin gelatin in PBST, and then incubated 1 h at 37 °C with the rabbit anti-StarD7Ct polyclonal (1:50) antibody. Cells were washed with PBST and incubated 1 h with Alexa Fluor 488-conjugated goat anti-rabbit IgG. Nuclei were stained with Hoechst 33258 dye. Cells were washed with PBST and slides were mounted in Aqueous Mounting Medium with fluorescent tracers (Fluor Save, Calbiochem). Cells were visualized in an epifluorescence microscope Nikon Eclipse TE 2000U (Nikon Corporation, Japan).

2.6. Transmission electron microscopy

HepG2 cells treated with siD7 or siC were cultured for 72 h. Then, cells were scraped, washed, and fixed in a mixture of 4% w/v formaldehyde and 1.5% w/v glutaraldehyde in 0.1 M cacodylate buffer plus 7% w/v sucrose for 2 h (Karnovsky fixative). Then, the cells were spun down by centrifugation, treated with 1% $OsS0_4$ for 1–2 h, dehydrated in an acetone series and embedded in Araldite. Thin sections were cut using a JEOL ultramicrotome with a diamond knife, stained with uranyl acetate and lead citrate and examined in a Zeiss LEO 906-E electron microscope.

2.7. Analysis of cell death

HepG2 cells transfected with either siC (control) or siD7 (silenced) during 72 h were suspended in PBS and stained with Annexin V-APC/propidium iodide (PI) according to manufacturer's protocol (BD Pharmingen). Control and silenced cells were detected and quantified by flow cytometry in a FACSCanto II flow cytometer (Becton-Dickinson).

2.8. MTT colorimetric assay

The viability of H_2O_2-treated cells was measured by the 3-(4,5-dimethylthiazol-2yl)-2, 5-diphenyltetrazolium bromide (MTT) assay. HepG2 cells were transfected with siD7 or siC in 96-well plates (1.5×10^4 cells/well). After 48 h of transfection, cells were incubated with H_2O_2 at different concentrations for 16 h. Then, MTT solution (5 mg/mL) was added to the culture medium (1:10) and incubated for 2.5 h (37 °C). After the incubation, the medium was removed and the precipitated dye was dissolved in 100 μL of DMSO. The O.D. (540 nm) was measured and results were expressed as percentage of cell viability relative to the untreated control. Three independent experiments were carried out in quadruplicates.

2.9. Detection of ROS generation

Intracellular ROS production in live cells was detected using the fluorogenic probe 2′,7′-dichlorodihydrofluorescein diacetate (H2DCFDA). HepG2 cells transfected with siRNAs during 48 h were

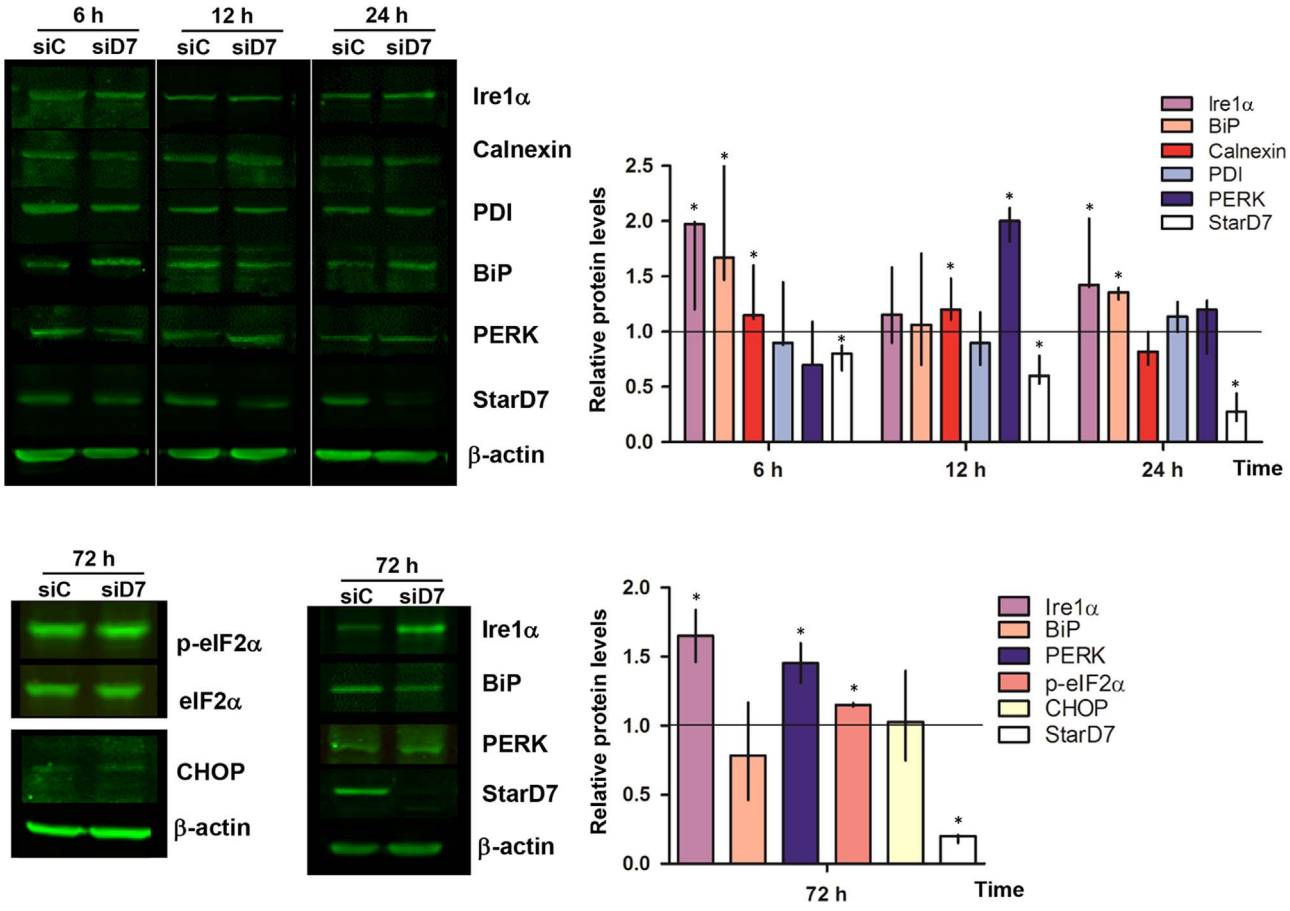

Fig. 3. Downregulation of StarD7 promotes ER response. Western blots analysis of IRE1α, Grp78/BiP, calnexin, PDI, PERK, p-eIF2α, total eIF2α, CHOP and StarD7 in protein extracts (100 μg/lane) from siC- or siD7-transfected cells after 6, 12, 24, or 72 h, as indicated. β-actin was used as a loading control. The graphs represent the densitometric analysis of the expression level of the indicated proteins in siD7-transfected cells normalized to β-actin expression of at least three independent experiments, and expressed relative to the corresponding normalized level in siC-transfected cells defined as 1, for each time after transfection. Values are median and 25th–75th percentiles of three experiments. *Statistically significant difference from control ($p < 0.01$).

grown 16 h in the presence of 0, 100, 200, or 300 μM H_2O_2, and then changed to media without phenol red (Invitrogen). Cells were incubated with 10 μM of H2DCFDA for 1 h at 37 °C. Then, the cells were washed with PBS (three times), placed on ice, and immediately analyzed by flow cytometry (FACSCanto II, Becton-Dickinson). The fluorescence signal was measured in viable cells.

2.10. Catalase enzyme activity

Catalase activity of fresh sonicated cell extracts was determined by measuring the continuous decrease in H_2O_2 absorbance at 240 nm ($\varepsilon = 40\ mM^{-1}\ cm^{-1}$) according to Beers and Sizer [24]. To this end, 50 or 100 μg of protein extracts from cells untransfected or transfected with siC or siD7 for 72 h, were incubated in 1 mL final volume of 20 mM H_2O_2 in PBS (50 mM, pH 7.0). The enzyme activity was measured in a quartz cuvette at 25 °C and expressed as U/mg of protein.

2.11. Statistical analysis

Significant differences for control and test conditions were identified using the nonparametric paired Wilcoxon test or unpaired Mann-Whitney U test. A Kruskal–Wallis with a Dunn's post-test was performed for multiple comparisons of independent samples. Statistically significant differences were considered for $p < 0.01$.

3. Results

3.1. Effects of StarD7 siRNA on HepG2 cell ultrastructure

siRNA gene silencing was used to deplete the expression of StarD7 and to determine its effect on cell ultrastructure. Compared with a non-targeting control siRNA (siC), treatment of HepG2 cells transfected for 72 h with two different specific siRNAs targeting human StarD7 mRNA (siD7 and siD7.2) resulted in a marked depletion of StarD7 protein (Fig. 1A and C). Accordingly, the expression of StarD7 mRNA was reduced by 80% in StarD7 knockdown cells (Fig. 1B). No changes in StarD7 levels were observed in siC cells compared to non-transfected HepG2 cells (Fig. 1A and B). Since both StarD7 siRNAs had similar silencing efficiency, the following experiments were performed with siD7.

Next, StarD7-silenced HepG2 cells were analyzed by transmission electron microscopy (EM) in order to study the effects of siD7 on cell ultrastructure. EM micrographs revealed that the mitochondria of StarD7-silenced cells were bigger and exhibited distorted cristae structure compared to siC control cells. In addition, the ER network was altered, often dilated (Fig. 2) and highly reminiscent of the morphological changes typically observed during the ER stress response.

3.2. Downregulation of StarD7 promotes ER response

To determine whether StarD7 deficiency promoted ER stress, we examined the expression of the main proteins involved in the

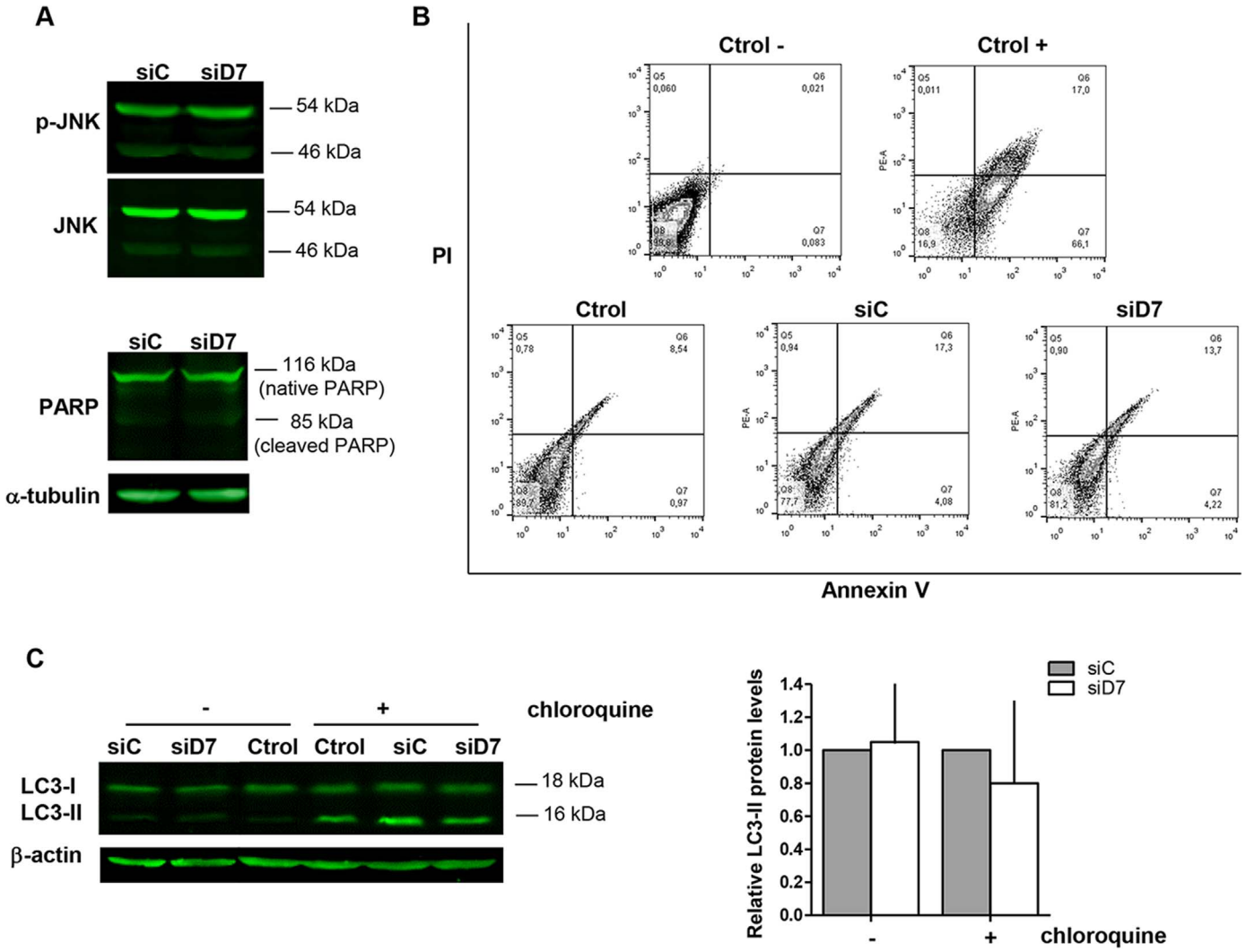

Fig. 4. StarD7 knockdown does not induce apoptosis activation. (A) PARP and phosphorylated JNK protein levels in StarD7 silenced HepG2 cells. HepG2 cells were transfected with siC or siD7 for 72 h. The expression levels were assayed by western blot using anti-PARP, anti-p-JNK, or anti-JNK antibodies and anti-α-tubulin as loading control. (B) Cells transfected with siC or siD7 for 72 h were processed and analyzed by flow cytometry as indicated in material and methods. PI was used to differentiate apoptotic cells with preserved membrane integrity (Annexin-V$^+$ PI$^-$) from those that had lost their membrane integrity (Annexin-V$^+$ PI$^+$). Density-plot diagrams of Annexin-V/PI labeled cells are shown. Negative (Ctrol$^-$ no staining cells) and positive (Ctrol$^+$ cells incubated at −80 °C for 15 min) controls are shown (upper plots). HepG2 cells without transfection (Ctrol), transfected with siC or with siD7 are shown in the bottom plots. (C) StarD7 knockdown does not induce autophagy activation. LC3-I and LC3-II expression were examined by immunoblot in non-transfected HepG2 cells (Ctrol) and cells transfected with siC or siD7 for 72 h treated or not with chloroquine (5 μM) for 24 h. The bar graph represents the densitometric quantification of LC3-II in siD7-transfected cells normalized to β-actin of at least three separate experiments and expressed relative to the corresponding normalized levels in siC-transfected cells defined as 1 (median and 25th–75th percentiles).

UPR pathway. To this end, HepG2 cells were transfected with siC or siD7 and protein extracts were obtained at 6, 12, 24, and 72 h post-silencing. Fig. 3 shows the protein expression levels of IRE1α, calnexin, PDI (protein disulfide isomerase), Grp78/BiP, PERK, eIF2α, p-eIF2α, C/EBP homologous protein (CHOP), and StarD7 in siD7-transfected cells relative to the corresponding levels in siC-transfected cells at each time. A significant time-dependent down-regulation of StarD7 levels was observed as early as 6 h after transfection (StarD7 half-life is less than 4 h -data not shown-). At six hours after StarD7 silencing, higher amounts of IRE1α and Grp78/BiP proteins were detected in siD7 cells compared to siC cells. In addition a slight increase in calnexin levels was detected at 6 and 12 h. Grp78/BiP returned to basal levels after 72 h of siD7-treatment. In contrast, IRE1α remained increased compared to control during all the times analyzed, whereas no significant changes in PDI and CHOP protein levels were detected. Moreover, the levels of PERK protein, a kinase whose active homodimer phosphorylates and inactivates eIF2α shutting off protein translation globally and reducing protein load on the ER, increased at 12 h in siD7 cells compared to siC cells and remained increased after 72 h. Consequently, a modest but significant phosphorylation of eIF2α was detected at 72 h post siD7 transfection.

Additionally, in order to explore whether StarD7 knockdown induces apoptosis, we measured the protein levels of poly(ADP-ribose) polymerase (PARP) and JNK. Fig. 4A indicates that these markers of apoptosis activation did not change when HepG2 cells were treated for 72 h with siD7 compared to siC cells. Moreover, PI/Annexin V levels measured by flow cytometry revealed no changes in siD7-treated cells relative to siC cells or untreated HepG2 cells (Fig. 4B).

Next, we explored whether siD7 induces autophagy. To this end, we determined the conversion of the mammalian protein LC3-I to the autophagosome-associated LC3-II which is considered the hallmark of autophagy [25]. Cells transfected with siC or siD7 for 72 h, or non-transfected cells were incubated in the presence/absence of the lysosome inhibitor chloroquine (5 μM) for additional 24 h. In these conditions, the levels of LC3-II remained unchanged, suggesting that autophagy is not induced in siD7-treated

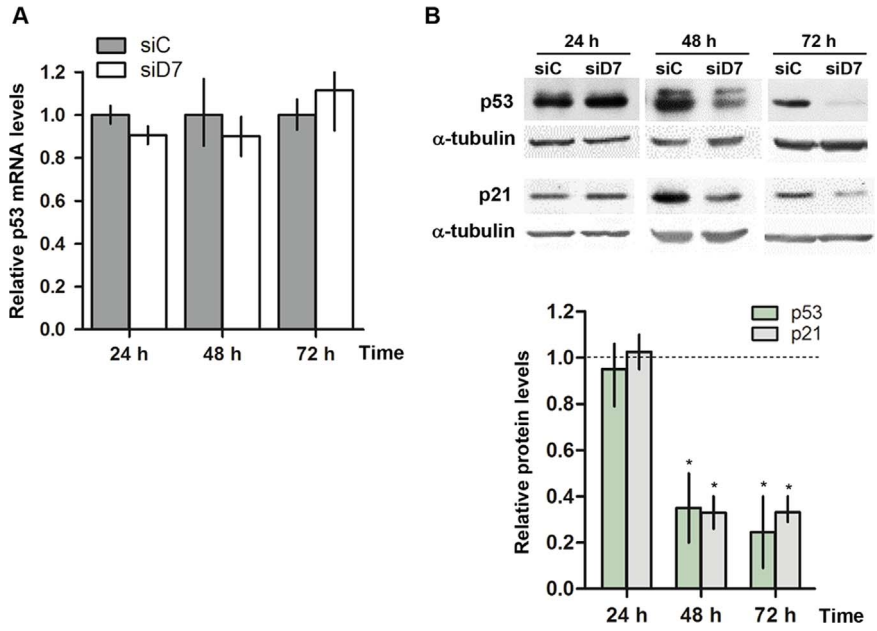

Fig. 5. StarD7 silencing reduces p53 and p21 expression level. HepG2 cells were transfected with siC or siD7 and cultured as indicated. (A) p53 mRNA expression was determined by qRT-PCR. Results are expressed as fold changes in p53 expression levels after normalizing to cyclophilin A relative to the corresponding normalized mRNA levels in siC-transfected cells. The values represent the median and 25th–75th percentiles of at least three independent experiments performed by triplicate. (B) p53 and p21 protein expression levels from siC- or siD7-transfected cells were analyzed by western blot. The graph represents the densitometric analysis of the protein expression levels in siD7-transfected cells normalized to α-tubulin expression of three independent experiments, and expressed relative to the corresponding normalized level in siC-transfected cells defined as 1, for each time after transfection. Values are median and 25th–75th percentiles of three experiments. *Statistically significant difference from control ($p < 0.01$).

cells (Fig. 4C).

Altogether, these results indicate that StarD7 silencing promotes an early response of proteins involved in maintaining the ER homeostasis. In addition, neither apoptosis nor autophagy was induced by StarD7 downregulation up to 72 h of StarD7 silencing.

3.3. StarD7 silencing promotes destabilization of p53

Considering that p53 is a tumor suppressor that plays a major role regulating cellular response to different stressors we examined whether HepG2 cells treated with siD7 modifies p53 expression by measuring mRNA and protein levels. qRT-PCR indicated that p53 mRNA levels were not affected by StarD7 siRNA treatment respect to siC (Fig. 5A). In contrast, we observed that p53 protein levels were significantly decreased in siD7 cells after 48 and 72 h, as it was the case for p21, whose gene is a target of p53 (Fig. 5B). These observations suggest that silencing of StarD7 is associated with changes in p53 protein stability. To address this, cells were transfected for 72 h with siC or siD7 and p53 protein levels were measured at different time points after treatment with 20 μg/mL cycloheximide, a known inhibitor of protein biosynthesis. Western blot assays revealed that p53 levels dropped earlier in siD7-transfected cells than in siC-transfected cells (Fig. 6A), suggesting that StarD7 silencing leads to a decrease in p53 stability. We further investigated this phenomenon by measuring p53 levels in siD7-treated cells in the presence/absence of the proteasome inhibitor MG132. We noticed that the downregulation of p53 protein levels in siD7-treated HepG2 cells was prevented when cells were treated with 10 μM MG132 during 4 h (Fig. 6B). These results indicate that StarD7 silencing decreases p53 half-life through a proteasome degradation mechanism. Moreover, these observations suggest that ER stress induced by StarD7 siRNA promotes the destabilization of p53 and consequently diminishes p21 protein expression.

3.4. StarD7 silencing induces ROS production

Taking into account that there is a cross-talk between ER stress and the cellular oxidative stress response [26], we tested whether siD7 modifies redox balance by measuring ROS levels. To this end, siD7- and siC-transfected HepG2 cells for 72 h were loaded for 1 h with 10 μM H2DCFDA, a membrane permeable non-fluorescent dye that is cleaved by intracellular esterases. Once cleaved, H2DCFDA reacts with ROS to produce a green fluorescence signal. It should be noted that H2DCFDA fluorescence is primarily due to the interaction of the dye with H_2O_2 or peroxyl products [27]. The quantification of ROS levels by flow cytometry showed increased H2DCFDA fluorescence signal in cells transfected with siD7 in comparison to siC-transfected cells or non-transfected cells (Fig. 7A). ROS levels in siD7 HepG2 cells were approximately 40% higher than those observed in siC cells (Fig. 7B). Since the basal ROS production increase could challenge cell capacity to survive when they are exposed to an injury we explored cell viability in siD7 compared to siC-transfected cells exposed to increasing H_2O_2 concentrations. These results indicate that the survival of StarD7-silenced HepG2 cells treated with different amounts of H_2O_2 for 16 h was significantly decreased in comparison to cells transfected with siC (IC50 of 278.6 μM for siD7 and IC50 of 444.7 μM for siC) (Fig. 7C).

Considering that PERK pathway also activates the expression of genes encoding antioxidant and oxidant-detoxifying enzymes [28], we explored the expression levels of HO-1 and catalase enzymes in siD7- and siC-transfected cells for 48 or 72 h. As shown in Fig. 7D, decreased StarD7 expression was associated to increased levels of the HO-1 and catalase proteins. Additionally, we observed increased catalase enzyme activity (H_2O_2 scavenger) in siD7-transfected cells at 72 h (Fig. 7E). These data point out that downregulation of StarD7 correlates with increased ROS levels and activation of an antioxidant defense response.

Altogether, these findings indicate that StarD7 modulates the oxidative balance probably by protecting cells from ROS-mediated toxicity.

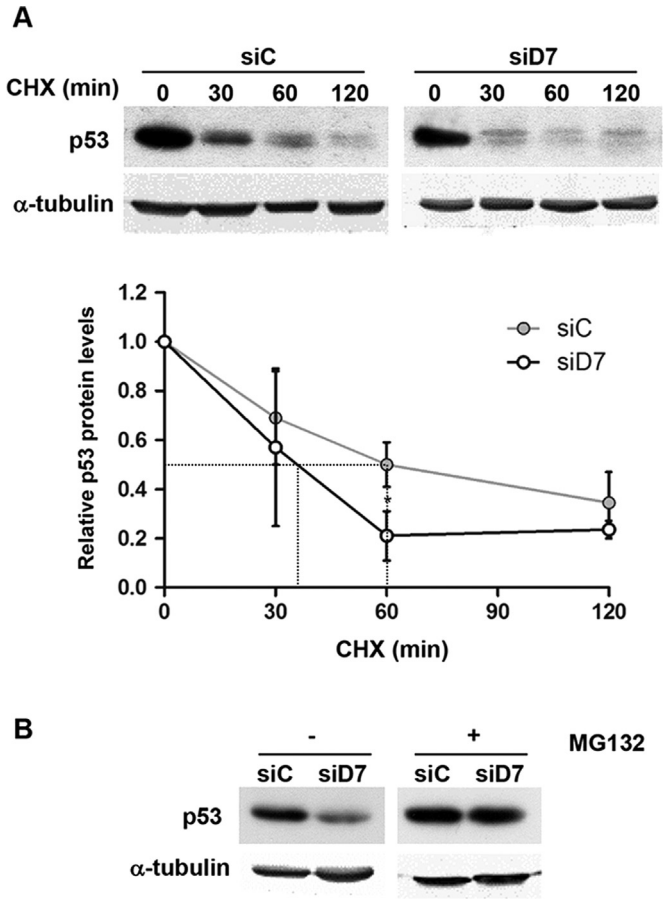

Fig. 6. StarD7 siRNA promotes destabilization of p53. (A) HepG2 cells were transfected with siC or siD7 for 72 h. Cells were treated with cycloheximide (CHX, 20 μg/mL) for the indicated hours, and western blots were performed. The graph represents the level of remaining p53 protein at each time points normalized to α-tubulin expression and depicted relative to the initial levels (0 h of CHX treatment) quantified in siC- or siD7-transfected cells, respectively. (B) HepG2 cells were transfected with siC or siD7 for 72 h and then treated or not with MG132 (10 μM) during 4 h. p53 expression levels were assayed by western blot.

4. Discussion

This study demonstrates that the depletion of StarD7 in HepG2 cells: (i) leads to alterations in mitochondria and ER morphology; (ii) causes ER stress response without alterations in apoptosis or authophagy markers; (iii) promotes the destabilization of p53; (iv) stimulates ROS generation in basal conditions; (v) reduces cell viability after H_2O_2 exposure; and (vi) increases HO-1 and catalase expression levels as well as catalase enzyme activity.

Alterations in the phospholipid metabolism, changes in the redox status and in intraluminal calcium levels, as well as the inability to perform post-translational modification of proteins leads to the activation of the ER stress response [29,30]. In this regard, it is well-known that PC depletion affects ER morphology [12]. In a previous study, we reported a decrease in phospholipids biosynthesis in cells treated with siD7 [6]. Here, we explored the consequences of StarD7 depletion on ER homeostasis and ROS production.

HepG2 cells treated with siRNA against StarD7 showed ultrastructural changes evidenced by a dilated rough ER and distorted mitochondrial cristae, compatible with an ER stress. Indeed, StarD7 silencing triggered the UPR pathway, which is supported by changes in the expression of proteins involved in UPR sensing and signaling: IRE1α, calnexin, Grp78/BiP, PERK, and p-eIF2α.

In addition, our study demonstrated that StarD7 siRNA induces a decrease in p53 half-life mediated by an increase in p53 degradation. Several reports have previously suggested a link between ER stress and p53 [16–21,31]. Interestingly, it has been proposed that ER stress prevents the pro-apoptotic function of p53 by enhancing its nucleo-cytoplasmic export and degradation as a mechanism of cell adaptation to ER stress induced by pharmacological or physiological means [16,17]. In line with this, ER stress induced by StarD7 siRNA may be alleviated by the decreased stability of p53. This is supported by the fact that no modifications in PARP, JNK and annexin V staining were observed indicating that the apoptotic program was not initiated. Additionally, no alteration in the levels of LC3-II, a hallmark of autophagy, was observed either with or without the addition of the lysosomal inhibitor chloroquine.

Also, StarD7 silencing led to the activation of PERK pathway as well as to the increase in basal ROS levels and the antioxidant HO-1 and catalase enzymes. These enzymes are known to play a central role in the defense against oxidative insults [32]. Consistently, it was reported that the PERK pathway not only attenuates global protein translation, but also activates the expression of genes encoding antioxidant and oxidant-detoxifying enzymes, such as HO-1 and glutathione S-transferase [28].

Taken together our results are in line with several studies that demonstrate a close relationship between ER stress and the oxidative stress response showing that basal ROS levels, necessary to perform normal signaling, increase after exposure to various forms of stress [33].

The specific mechanism by which the siRNA against StarD7 impacts on cellular redox homeostasis is unknown at present. However, it might be related to its ability to transport PC. Mitochondria lack the ability to synthesize PC, thus import of this phospholipid is likely critical for mitochondrial homeostasis [34,35]. Experimental evidences showed a clear relationship between mitochondrial dysfunction, decreased PC, increased ROS and oxidized PC levels [36,37]. Similarly to StarD1 and StarD4, which transport cholesterol and cholesterol hydroperoxide species, StarD7 might transport not only PC but also oxidized PC [38,39]. Therefore, it is possible to hypothesize that StarD7 knockdown leads to decreased PC in mitochondria or to the accumulation of oxidized PC in sensitive intracellular compartments, which results in increased ROS, HO-1 and catalase levels as well as increased p53 degradation. Moreover, the accumulated oxidized PC species might in turn make cells more sensitive to H_2O_2 treatment. Indeed, our results indicate that StarD7 knockdown increases cell susceptibility to oxidative injury observed as reduced cell viability upon treatment with H_2O_2. Consistently, it was reported that oxidized PC induced a decrease in p53 levels in HepG2 cells without altering p-JNK or caspase 3, but cell viability was markedly reduced when the cells were treated with oxidized PC plus an inhibitor of GSH production [40].

On the other hand, there is increased evidence that lipid transfer proteins transport lipids at membrane contact sites. One of these special domains for interaction is the mitochondria-associated membrane (MAM) that provides a platform for lipid synthesis and lipid transfer between ER and mitochondria [41]. During cellular stress, a group of MAM-regulatory proteins is altered, thus leading to changes in MAM functions [42]. Therefore, it is possible to speculate that StarD7 depletion may cause alterations in MAMs due to altered PC transport, resulting in oxidative stress and p53 degradation.

In summary, this study reveals that the loss of StarD7 protein results in altered ER and mitochondria morphology, and initiates the UPR pathway concomitantly with an increased ROS generation and antioxidant response. These findings allow us to hypothesize that beyond its role in lipid transport StarD7 participates in cellular redox homeostasis.

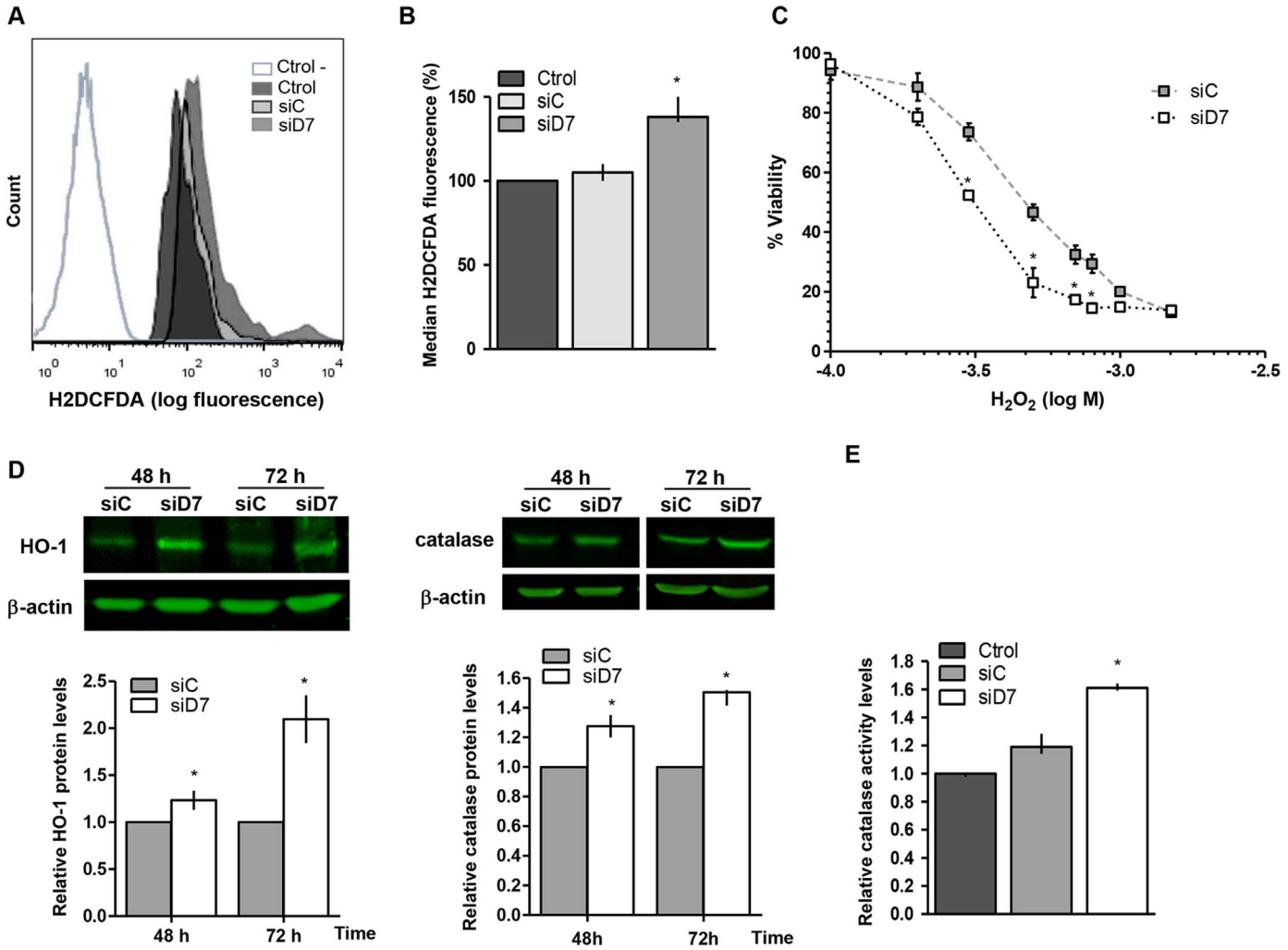

Fig. 7. StarD7 silencing induces ROS production and sensitizes cells to H_2O_2 exposure. (A) A representative histogram overlay denotes fluorescence signal in non-transfected (Ctrol), and siD7- or siC-transfected cells for 72 h and measured by flow cytometry. The negative control (Ctrol-) represents non transfected cells that were not incubated with H2DCFDA. (B) The bar graph represents the median H2DCFDA fluorescence in non-transfected and siD7- or siC-transfected cells for 72 h (median and 25th–75th percentiles $^*p < 0.01$). (C) siD7- and siC-transfected cells for 72 h were treated with different amounts of H_2O_2 concentrations and cell viability was determined by MTT assay and expressed as percentage respect to the corresponding values in untreated cells. IC50: 278.6 μM for siD7 *vs* 444.7 μM for siC (media ± SEM, n=8). $^*p < 0.01$ compared to siC-transfected cells. (D) HO-1 and catalase protein expression were analyzed by western blot using protein extracts (100 μg/lane) from siC- or siD7-transfected cells. The bar graph represents the densitometric quantification of HO-1 and catalase protein levels in siD7-transfected cells normalized to β-actin of at least three separate experiments, and expressed relative to the corresponding normalized protein levels in siC-transfected cells (median and 25th–75th percentiles). $^*p < 0.01$ compared to siC-transfected cells. (E) Catalase enzyme activity measured in non-transfected (Ctrol) and siC- or siD7-transfected cells for 72 h. The bar graph represents the catalase enzyme activity normalized to Ctrol (7.2 U/mg) defined as 1 of at least three separate experiments performed by duplicate (median and 25th–75th percentiles). $p < 0.01$ compared to Ctrol.

Acknowledgements

We gratefully acknowledge Drs. José Bocco, Lucas Trucco, Cecilia Sanchez and Miriam Virgolini for reagents and helpful advice. Also we are very grateful to Dr. Héctor Alex Saka for the correction of the manuscript.

This work was funded by the Consejo Nacional de Investigaciones Científicas y Tecnológicas de Argentina (CONICET), the Agencia Nacional de Promoción Ciencia y Técnica (FONCYT) PICT 2011-0452, and the Secretaría de Ciencia y Técnica de la Universidad Nacional de Córdoba (SECyT-UNC). S.G-R. and G.M.P-D. are Career Investigators of CONICET. J F-M, L-R, and M E-R thank FONCYT and CONICET for her fellowships.

References

[1] C.P. Ponting, L. Aravind, START: a lipid-binding domain in StAR, HD-ZIP and signalling proteins, Trends Biochem. Sci. 24 (1999) 130–132.
[2] F. Alpy, C. Tomasetto, START ships lipids across interorganelle space, Biochimie 96 (2014) 85–95.
[3] S. Durand, S. Angeletti, S. Genti-Raimondi, GTT1/StarD7, a novel phosphatidylcholine transfer protein-like highly expressed in gestational trophoblastic tumour: cloning and characterization, Placenta 25 (2004) 37–44.
[4] S. Angeletti, V. Rena, R. Nores, R. Fretes, G.M. Panzetta-Dutari, S. Genti-Raimondi, Expression and localization of StarD7 in trophoblast cells, Placenta 29 (2008) 396–404.
[5] Y. Horibata, H. Sugimoto, StarD7 mediates the intracellular trafficking of phosphatidylcholine to mitochondria, J. Biol. Chem. 285 (2010) 7358–7365.
[6] J. Flores-Martin, V. Rena, S. Marquez, G.M. Panzetta-Dutari, S. Genti-Raimondi, StarD7 knockdown modulates ABCG2 expression, cell migration, proliferation, and differentiation of human choriocarcinoma JEG-3 cells, PLoS One 7 (2012) e44152.
[7] V. Rena, J. Flores-Martín, S. Angeletti, G. Panzetta-Dutari, S. Genti-Raimondi, StarD7 gene expression in trophoblast cells: contribution of SF-1 and Wnt-b-catenin signalling, Mol. Endocrinol. 8 (2011) 1364–1375.
[8] Y. Ikeda, E. Tanji, N. Makino, S. Kawata, T. Furukawa, MicroRNAs associated with mitogen-activated protein kinase in human pancreatic cancer, Mol. Cancer Res. 10 (2011) 259–269.
[9] J. Flores-Martin, V. Rena, S. Angeletti, G.M. Panzetta-Dutari, S. Genti-Raimondi, The lipid transfer protein StarD7: structure, function, and regulation, Int. J. Mol. Sci. 14 (2013) 6170–6186.
[10] L. Yang, I. Lewkowich, K. Apsley, J.M. Fritz, M. Wills-Karp, T.E. Weaver, Haploinsufficiency for Stard7 is associated with enhanced allergic responses in lung and skin, J. Immunol. (2015).

[11] M.H. van der Sanden, M. Houweling, L.M. van Golde, A.B. Vaandrager, Inhibition of phosphatidylcholine synthesis induces expression of the endoplasmic reticulum stress and apoptosis-related protein CCAAT/enhancer-binding protein-homologous protein (CHOP/GADD153), Biochem. J. 369 (2003) 643–650.
[12] N. Testerink, M.H. van der Sanden, M. Houweling, J.B. Helms, A.B. Vaandrager, Depletion of phosphatidylcholine affects endoplasmic reticulum morphology and protein traffic at the Golgi complex, J. Lipid Res. 50 (2009) 2182–2192.
[13] E. Lai, T. Teodoro, A. Volchuk, Endoplasmic reticulum stress: signaling the unfolded protein response, Physiology 22 (2007) 193–201.
[14] K.M. Ryan, A.C. Phillips, K.H. Vousden, Regulation and function of the p53 tumor suppressor protein, Curr. Opin. Cell Biol. 13 (2001) 332–337.
[15] M. Oren, Decision making by p53: life, death and cancer, Cell Death Differ. 10 (2003) 431–442.
[16] L. Qu, S. Huang, D. Baltzis, A.M. Rivas-Estilla, O. Pluquet, M. Hatzoglou, C. Koumenis, Y. Taya, A. Yoshimura, A.E. Koromilas, Endoplasmic reticulum stress induces p53 cytoplasmic localization and prevents p53-dependent apoptosis by a pathway involving glycogen synthase kinase-3beta, Genes Dev. 18 (2004) 261–277.
[17] O. Pluquet, L.K. Qu, D. Baltzis, A.E. Koromilas, Endoplasmic reticulum stress accelerates p53 degradation by the cooperative actions of Hdm2 and glycogen synthase kinase 3beta, Mol. Cell Biol. 25 (2005) 9392–9405.
[18] J.N. Gass, N.M. Gifford, J.W. Brewer, Activation of an unfolded protein response during differentiation of antibody-secreting B cells, J. Biol. Chem. 277 (2002) 49047–49054.
[19] N. Dioufa, I. Chatzistamou, E. Farmaki, A.G. Papavassiliou, H. Kiaris, p53 antagonizes the unfolded protein response and inhibits ground glass hepatocyte development during endoplasmic reticulum stress, Exp. Biol. Med. 237 (2012) 1173–1180.
[20] W.C. Lin, Y.C. Chuang, Y.S. Chang, M.D. Lai, Y.N. Teng, I.J. Su, C.C. Wang, K.H. Lee, J.H. Hung, Endoplasmic reticulum stress stimulates p53 expression through NF-kappaB activation, PLoS One 7 (2012) e39120.
[21] I. Lopez, A.S. Tournillon, K. Nylander, R. Fahraeus, p53-mediated control of gene expression via mRNA translation during Endoplasmic Reticulum stress, Cell Cycle 14 (2015) 3373–3378.
[22] T. Namba, K. Chu, R. Kodama, S. Byun, K.W. Yoon, M. Hiraki, A. Mandinova, S. W. Lee, Loss of p53 enhances the function of the endoplasmic reticulum through activation of the IRE1alpha/XBP1 pathway, Oncotarget 6 (2015) 19990–20001.
[23] V. Litvak, Y.D. Shaul, M. Shulewitz, R. Amarilio, S. Carmon, S. Lev, Targeting of Nir2 to lipid droplets is regulated by a specific threonine residue within its PI-transfer domain, Curr. Biol. 12 (2002) 1513–1518.
[24] R.F. Beers Jr., I.W. Sizer, A spectrophotometric method for measuring the breakdown of hydrogen peroxide by catalase, J. Biol. Chem. 195 (1952) 133–140.
[25] G. Kroemer, G. Marino, B. Levine, Autophagy and the integrated stress response, Mol. Cell 40 (2010) 280–293.
[26] B. Bhandary, A. Marahatta, H.R. Kim, H.J. Chae, An involvement of oxidative stress in endoplasmic reticulum stress and its associated diseases, Int J. Mol. Sci. 14 (2012) 434–456.
[27] A.S. Keston, R. Brandt, The fluorometric analysis of ultramicro quantities of hydrogen peroxide, Anal. Biochem. 11 (1965) 1–5.
[28] R. Inagi, Endoplasmic reticulum stress in the kidney as a novel mediator of kidney injury, Nephron Exp. Nephrol. 112 (2009) e1–e9.
[29] S. Fu, L. Yang, P. Li, O. Hofmann, L. Dicker, W. Hide, X. Lin, S.M. Watkins, A. R. Ivanov, G.S. Hotamisligil, Aberrant lipid metabolism disrupts calcium homeostasis causing liver endoplasmic reticulum stress in obesity, Nature 473 (2011) 528–531.
[30] T.A. Lagace, N.D. Ridgway, The role of phospholipids in the biological activity and structure of the endoplasmic reticulum, Biochim. Biophys. Acta 1833 (2013) 2499–2510.
[31] K. Bourougaa, N. Naski, C. Boularan, C. Mlynarczyk, M.M. Candeias, S. Marullo, R. Fahraeus, Endoplasmic reticulum stress induces G2 cell-cycle arrest via mRNA translation of the p53 isoform p53/47, Mol. Cell 38 (2010) 78–88.
[32] L.E. Fredenburgh, M.A. Perrella, S.A. Mitsialis, The role of heme oxygenase-1 in pulmonary disease, Am. J. Respir. Cell Mol. Biol. 36 (2007) 158–165.
[33] K. Zhang, Integration of ER stress, oxidative stress and the inflammatory response in health and disease, Int. J. Clin. Exp. Med. 3 (2010) 33–40.
[34] J.E. Vance, Phospholipid synthesis and transport in mammalian cells, Traffic 16 (2015) 1–18.
[35] L.C. Schenkel, M. Bakovic, Formation and regulation of mitochondrial membranes, Int. J. Cell Biol. 2014 (2014) 709828.
[36] D. Gao, F. Jin, H. Liu, Y. Wang, Y. Jiang, Metabonomic study on the antitumor effect of flavonoid derivative 3d in HepG2 cells and its action mechanism, Talanta 118 (2014) 382–388.
[37] X. Shao, D. Gao, Y. Wang, F. Jin, Q. Wu, H. Liu, Application of metabolomics to investigate the antitumor mechanism of flavopiridol in MCF-7 breast cancer cells, J. Chromatogr. B Anal. Technol. Biomed. Life Sci. 1025 (2016) 40–47.
[38] W. Korytowski, K. Wawak, P. Pabisz, J.C. Schmitt, A.W. Girotti, Macrophage mitochondrial damage from StAR transport of 7-hydroperoxycholesterol: implications for oxidative stress-impaired reverse cholesterol transport, FEBS Lett. 588 (2013) 65–70.
[39] W. Korytowski, D. Rodriguez-Agudo, A. Pilat, A.W. Girotti, StarD4-mediated translocation of 7-hydroperoxycholesterol to isolated mitochondria: deleterious effects and implications for steroidogenesis under oxidative stress conditions, Biochem. Biophys. Res. Commun. 392 (2010) 58–62.
[40] Y. Suzuki, K. Nakagawa, S. Kato, N. Tatewaki, S. Mizuochi, J. Ito, T. Eitsuka, H. Nishida, T. Miyazawa, Metabolism and cytotoxic effects of phosphatidylcholine hydroperoxide in human hepatoma HepG2 cells, Biochem. Biophys. Res. Commun. 458 (2015) 920–927.
[41] J.C. Holthuis, A.K. Menon, Lipid landscapes and pipelines in membrane homeostasis, Nature 510 (2014) 48–57.
[42] A. Raturi, T. Simmen, Where the endoplasmic reticulum and the mitochondrion tie the knot: the mitochondria-associated membrane (MAM), Biochim. Biophys. Acta 1833 (2013) 213–224.